



BABEŞ-BOLYAI UNIVERSITY,
FACULTY OF PHYSICS

UNIVERSITE DE GRENOBLE,
ECOLE DOCTORALE DE PHYSIQUE

DOCTORATE THESIS REVIEW

Synthesis and Characterization of $Pb(V_{1-x}M_x)O_3$ (M = Ti, Fe) compounds

Scientific supervisors

Prof.dr. Aurel Pop
Babeş-Bolyai University, Cluj-Napoca
Prof.dr. Pierre Bordet
Néel Institute, CNRS, Grenoble, France

Student

Alexandru Okos

MMXIII

Synthesis and Characterization of $Pb(V_{1-x}M_x)O_3$ (M = Ti, Fe) compounds

Objectives and motivation

Recently multiferroic compounds attracted huge interest due to their unique properties which make such materials very interesting for real life applications, from capacitors, sensors and actuators to computer memory devices. $PbVO_3$ is a very promising material. It is isostructural with $PbTiO_3$ which is a very well known and studied ferroelectric material and it also contains vanadium V^{4+} cations which carry a 1/2 spin so magnetic ordering can be expected. However, no sign of magnetic ordering could be observed which raises the following questions:

1) Why is $PbVO_3$ not magnetic?

2) Could it be tuned so that it becomes magnetic?

There are two main explanations proposed for the absence of a clearly visible overall magnetic moment despite the presence of the V^{4+} cations. The first explanation is that the formation of strongly covalent vanadyl bonds forming a 2D array in the (a,b) plane could lead to a 2D behaviour with a possibly reduced magnetic moment with the d1 electron of vanadium engaged in the covalent bonding. The second explanation is that the magnetic moments of vanadium form a frustrated magnetic network.

The objective of the project was to provide some answer to the above questions by studying the effects of the partial substitution of vanadium by titanium and iron. Considering the first explanation, replacing V by Ti or Fe should reduce the 2D character and might allow for 3D magnetic ordering to appear. Of course magnetic Fe cations would probably be more efficient for that purpose. In the hypothesis of frustration as the origin of the weak magnetic signal, disorder induced by the substitution could release the frustration and lead to magnetic ordering through the “order by disorder” phenomenon.

We prepared two kinds of samples, polycrystalline and single crystals. Single crystals were prepared only in the form of clean $PbVO_3$ in which no substitution was attempted. The polycrystalline batch is larger containing two series, the titanium series and the iron series with the chemical compositions as follows.

$PbV_{1-x}Ti_xO_3$ with x = 0, 0.1, 0.25, 0.5 0.6, 0.75, 0.8, 1

$PbV_{1-x}Fe_xO_3$ with x = 0.1, 0.25, 0.3, 0.4, 0.5, 0.55, 0.6 0.65, 0.75

The structure and the physical properties of the samples were studied and an attempt was made to correlate the results and try to formulate a model which could explain the intriguing and often apparently contradicting behaviours of our compounds. The present work discusses the results obtained during the study and attempts to shed some light on the subject, without asserting that it reaches a final and definitive conclusion.

The work is structured on five chapters.

The first chapter reviews the fundamental concepts of the physics behind the multiferroic compounds, emphasizing the exotic properties / phenomena that are connected to our compounds. The first chapter also deals with the data already published in literature for $PbVO_3$ and some substitution compounds.

The second chapter describes the experimental methods and investigation techniques used during the study.

The third chapter presents the preparation methods, the high pressure - high temperature equipments employed and the reaction conditions required for the synthesis of $PbVO_3$ (and the substitution counterparts). The discussion continues with the first investigations and results which are concerned with phase purity.

The fourth chapter discusses with somewhat greater details the structural properties of the samples.

The fifth chapter deals with the magnetic and dielectric properties of the $Pb(VM)O_3$ compounds.

Since the physical properties of these materials are strongly dependent on the structure of the samples, the chapters intertwine at times, in each chapter results from the other chapters being mentioned and some redundancy is thus unavoidable.

Keywords: $PbVO_3$, multiferroic compounds, high pressure synthesis, X-Ray and neutron diffraction, Raman, EPR, SQUID

Table of contents

Chapter I. Multiferroic $PbVO_3$ perovskite

I.1. Introduction to multiferroics

Multiferroics are materials which present at least two of the ferroic properties, namely ferromagnetism, ferroelectricity and ferroelasticity. The definition of multiferroic materials is extended to also include antiferromangetism and antiferroelectricity [1-3]. A better definition of a multiferroic material is therefore that of a material which presents two or more order parameters. A magneto-electric material on the other hand is a material for which the magnetization can be controlled with an electric field or the polarization can be controlled with a magnetic field.

The names awarded to these categories of materials can appear to be misleading but a representation with diagrams of the classes of materials discussed above helps to provide a clear image (figure 1.1).

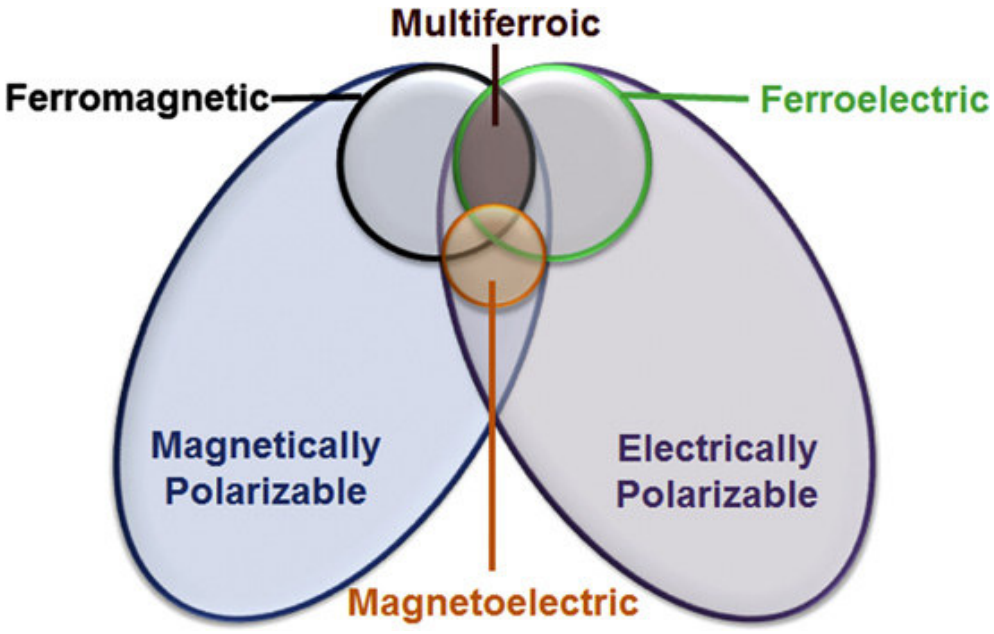

Fig. 1.1. Classification of multiferroic and magneto-electric materials [4].

There are two types of multiferroic materials, classified by their construction:

a) artificial multiferroics (or extrinsic multiferroics) are thin film hetero-structures composed of alternating layers of ferroelectric and ferromagnetic materials

b) single phase multiferroics (or intrinsic multiferroics) are materials in which the ferroelectric and ferromagnetic properties exist in the same phase [1, 2].

There are two types of coupling mechanisms between the ferroic properties in these materials.

The first type is observed for materials in which the ferroelectric and the magnetic orderings are associated to different sublattices. This type of coupling is generally weak but materials which present this type of coupling can have large values of the ferroelectric polarization [5, 6]. Multiferroics which display this mechanism are called type 1 or proper multiferroics.

The second type of coupling appears in materials for which the ferroelectric ordering is induced indirectly by a charge ordering or a magnetic ordering. This coupling is expected to be stronger because the electric dipoles can be directly switched by applying a magnetic field but the ferroelectric polarization is small for these materials [1, 5]. Multiferroics which display this mechanism are called type 2 or improper multiferroics.

I.2. Requirements for multiferroics

Generally, magnetic and ferroelectric type orderings are mutually exclusive. A multiferroic material must therefore contain properties which are conflicting by their own nature. The reasons for these conflicts are related to the crystal symmetry of the materials, to the electronic configurations of the ions that form the materials and to their conductive properties. In order for a material to be ferroelectric, it must crystallize in a non-centro-symmetric space group, but there are only a few space groups that are not centro-symmetric. For it to be ferromagnetic it must contain ions which carry a magnetic

moment. Usually, the magnetism in these magnetic ions is given by the presence of unpaired electrons in d orbitals, but, the presence of d orbitals tends to reduce the non-centro-symetric distortion, responsible for ferroelectricity. A ferroelectric material must be an electric insulator, otherwise the electric charges will redistribute, but most magnets are conductors.

Only a few compounds hold (anti)ferroelectricity and (anti)ferromagnetism. From these, type 1 intrinsic multiferroics are particularly interesting and promising for applications, due to their high spontaneous polarization. These are ABO_3 type perovskites. The ABO_3 type perovskite structure allows a wide range of possible oxidation states of the cations (for example $A^{2+}B^{4+}O_3$ or $A^{3+}B^{3+}O_3$) [3] and the possibility of tuning the properties of the material simply by substituting the cations on the A site or the B site [3]. One tuning possibility is to attempt to construct a material in which the A site cation (Pb, Bi,…) contains a stereochemically active lone electron pair and so is responsible for ferroelectric ordering and the B site cation (transition metal) contains partially filled d shells and therefore is responsible for magnetism [7-12]. $BiFeO_3$, $BiMnO_3$, $YCrO_3$, $PbVO_3$ are reported examples of such materials. $BiFeO_3$ is essentially the only single phase multiferroic that simultaneously posses ferroelectric ($T_C \approx 1100$ K) and antiferromagnetic ordering ($T_N \approx 643$ K) at RT [3, 5, 6].

I.3. Results reported on $PbVO_3$

The preparation of $PbVO_3$ was reported first in 2004 by Bordet et al. [13]. They synthesized $PbVO_3$ samples under HP-HT conditions from a mixture of PbO, PbO_2 and V_2O_3 at HP = 4.5 GPa, HT = 750° - 850° C and dwell times of 3 hours. Single phase samples were obtained at 825° C for a non-stoichiometric mixture corresponding to the composition of $PbVO_{2.8}$. They were also the first to solve the structure of $PbVO_3$ by XRD and NPD, to observe the absence of any magnetic signal from NPD and to discover the decomposition temperature of $PbVO_3$ (330°C).

Shpanchenko [14] prepared $PbVO_3$ samples using PbO and VO_2 as starting products and reaction conditions of HP = 40 – 80 kbars, temperatures of 650-1000° C and

dwell times of 5 to 240 minutes. Belik [15] prepared $PbVO_3$ samples under similar conditions and noticed that a re-annealing process greatly improves the quality of the samples. Other synthesis experiments on bulk $PbVO_3$ were conducted by Tsirlin [16], Oka [17] (who prepared single crystals by the hydrothermal method), Arévalo [18], Atahar [19] and Zhou [20] under various reaction conditions but the reactions conditions were always on the domain of high pressures, from 2GPa to 30 GPa. Arévalo tested the V-Ti substitution and Tsuchiya [31] prepared the $PbV_{1/2}Fe_{1/2}O_3$ compound again, under HP-HT conditions.

From literature, the structural data for $PbVO_3$ is the following: the sample belongs to the tetragonal system with the space group P4mm and the lattice parameters a = 3.8 Å and c = 4.67 Å. The Pb atom is at the origin of the system occupying the 1a (0, 0, 0) position and V is found in the off-centre position 1b (0.5, 0.5, 0.568). Oxygen atoms form a square pyramid with the apical oxygen O1 in 1b at (0.5, 0.5, 0.245) and the oxygen atoms forming the base, O2, at 2c (0.5, 0, 0.696).

Concerning the physical properties of this material, it is reported that $PbVO_3$ is a semiconductor [14] and it undergoes a phase transition under high pressure from a tetragonal semiconductor system to a cubic one characterized by metallic conductivity [15]. The ferroelectric polarization of $PbVO_3$ is predicted to be as high as $Ps = 1.6\ C*m^{-2}$. Magnetic susceptibility measurements (and μSR) reveal the presence of a magnetic transition. However, this transition is not detected by NPD or specific heat measurements.

Chapter II. Synthesis

II.1. HP-HT equipments

The downside of $PbVO_3$ but at the same time the thing that makes research so interesting is that it requires very high pressures for synthesis. Nobody so far was able to synthesise $PbVO_3$ bulk samples at ambient pressure [14].

Our samples were prepared by solid state reaction under high pressure – high temperature conditions (HP-HT). The best results were obtained in the range of 6 GPa and 950°C. The extreme pressure of 6 GPa is achieved by using two specially built devices. These are the CONAC press and the BELT X press. Figure 1.2 shows a schematic of the pressure cells used in the two machines.

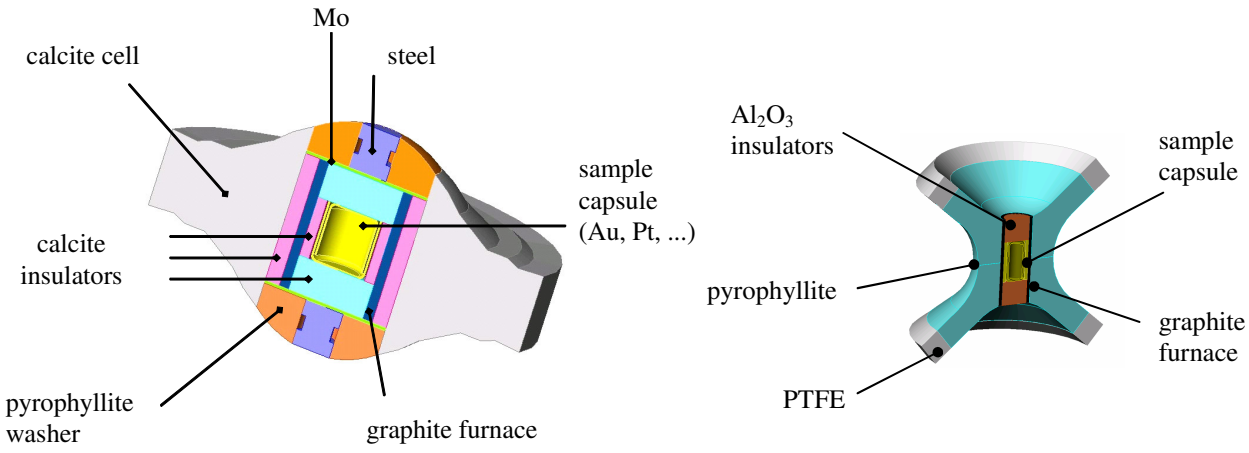

Fig. 2.1. CONAC pressure cell (left), BELT pressure cell (right).

The two machines work on the same principle. The starting oxides mixture is placed inside a Pt capsule which is then enclosed in the pressure cell. There are two plates (or anvils) for the CONAC press and two pistons for the BELT apparatus which apply a force to the pressure cell, thus creating the required pressure. A graphite cylinder is present in both cells. An electric current is passed through the plates/pistons of the press and through the graphite causing it to heat and act like a furnace. In this way the high temperature is achieved at the same time with the high pressure [21-23].

The samples were prepared from stoichiometric mixtures of PbO, PbO_2, V_2O_3, V_2O_5, TiO_2 and Fe_2O_3.

For the powder samples, the same reaction conditions were used for all the compositions. A diagram of the profile is presented in figure 2.2. The program was made of a dwell in pressure and in temperature at 6 GPa and 950° C for 90 minutes followed by a rapid quench and the release of pressure.

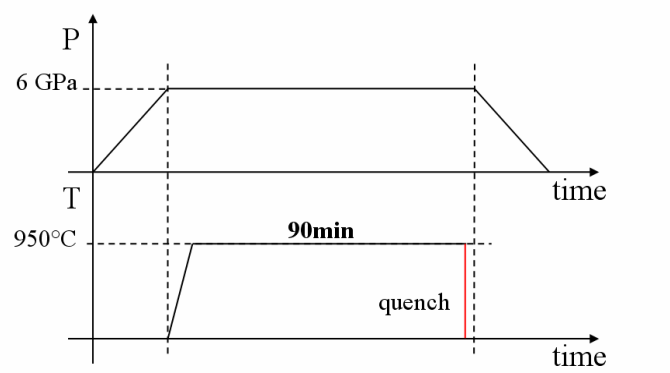

Fig. 2.2. Pressure and temperature dwells for powder samples.

For the preparation of single crystals we used the hydrothermal method as described in [17]. Again, the mixture of staring oxides was sealed in a Pt capsule but, unlike for the powder, 10 % wt of water was added to the mixture. The profile was also changed. Figure 2.3 shows the new program. The dwell time was reduced to 30 minutes and was followed by a slow cooling (while maintaining the pressure). After the final temperature was reached the sample was quenched and finally the pressure released.

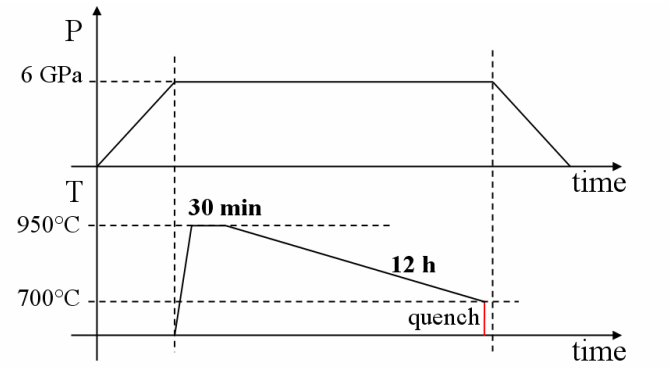

Fig. 2.3. Pressure and temperature program for single crystal growth.

II.2. The first results – phase characterization

At this stage XRD was used as the first investigation technique in order to confirm the formation of the required phase and the presence or absence of starting products and/or secondary phases in the final product. From these measurements it was observed that almost single phase samples were obtained both for the $PbVO_3$ composition and for the substitution series.

In the case of $PbVO_3$ a re-annealing treatment was found to provide samples of higher purity. Figure 2.4 shows the XRD pattern / Rietveld refinement for the best $PbVO_3$ sample (after the re-annealing process). The red points are the experimental data, the diagram recorded by the diffractometer. The black line is the calculated diagram. The rows of ticks mark the positions of the Bragg reflections from the phases taken in the calculated diagram. Lastly, the blue line is the difference between the observed and calculated diagrams.

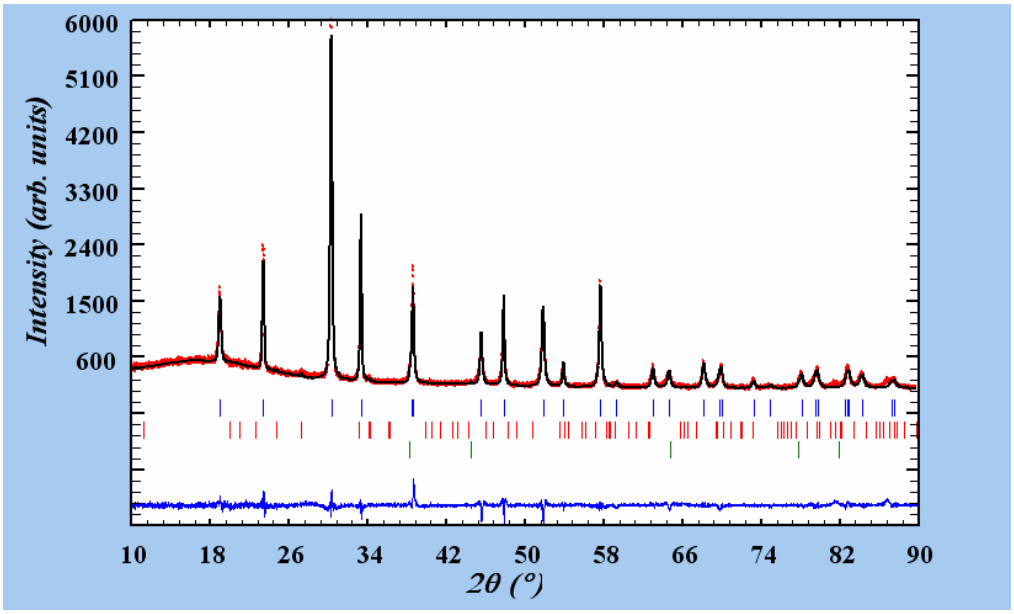

Fig. 2.4. $PbVO_3$ sample after re-annealing at HP-HT 6 GPa / 950 °C / 90 min.

The main phase (blue tics) is identified as $PbVO_3$ and is indexed with data available in literature [14] namely, a tetragonal structure with the space group P4mm, lattice parameters a = b = 3.8 Å and c = 4.67 Å. The other two phases are identified as hydrocerussite, $Pb_3(CO_3)_2(OH)_2$ [24] (the second row of ticks) and gold (third row of

ticks). The estimated percentage of hydrocerussite in the sample is approximately 2.8 %, however since this value is under the roughly 5% limit, it can not be considered a reliable value.

$PbVO_3$ single crystals were also prepared. The average lengths of the crystals are between 100 to 500 µm and the width of the crystals is approximately 50 µm, in agreement with the literature [17].

For the Ti substitution samples or Fe substitution samples (with less than 50% Fe) there is no need for re-annealing. Some examples of XRD patterns (and the subsequent Rietveld refinements) are provided for both substitution types on figure 2.5 and figure 2.6.

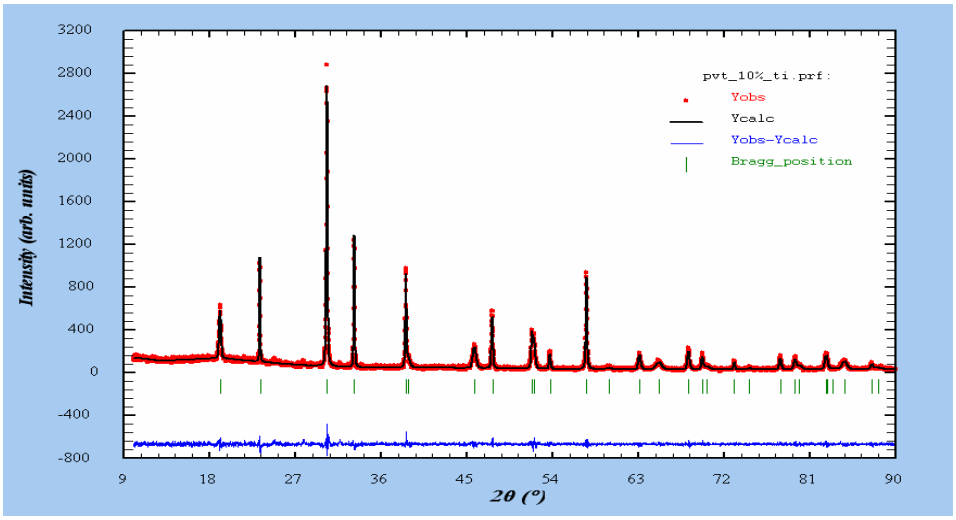

Fig. 2.5. XRD and Rietveld refinement for $PbV_{0.9}Ti_{0.1}O_3$.

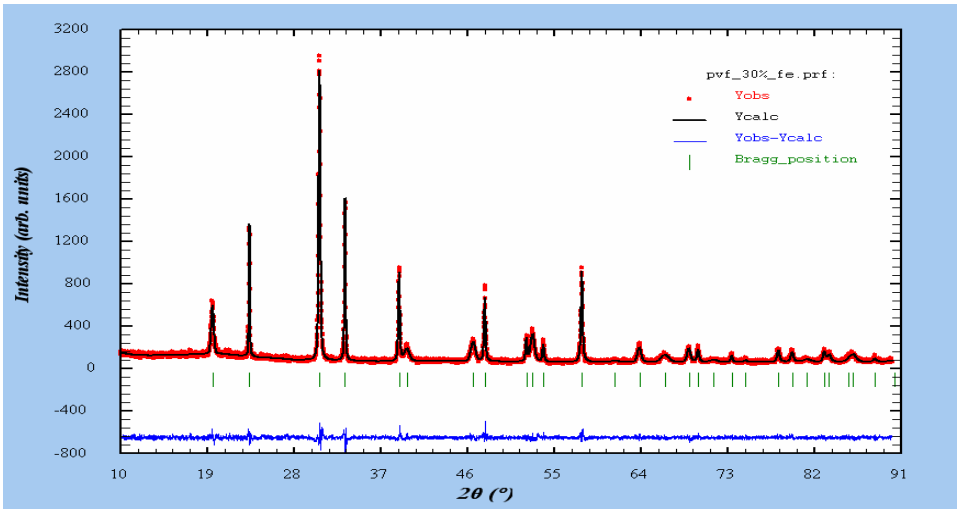

Fig. 2.6. XRD and Rietveld refinement for $PbV_{0.7}Fe_{0.3}O_3$.

The chemical composition and homogeneity of the cation distribution were verified by EDX. It was found that the observed composition is very close to the nominal composition (within the esd's of the EDX setup) and that the distribution is homogenous.

The oxidation states of vanadium for four representative samples were determined from X-Ray absorption spectroscopy measurements performed at the BM32 FAME French CRG beamline at the ESRF synchrotron facility in Grenoble, France. The representative samples were the following: $PbVO_3$, $PbV_{0.75}Ti_{0.25}O_3$ (25% Ti), $PbV_{0.75}Fe_{0.25}O_3$ (25% Fe) and $PbV_{0.5}Fe_{0.5}O_3$ (50% Fe). The oxidation state was determined from the position of the absorption pre-peak of the V k edge. This peak is located at about 5470 eV. A zoom on the pre-peak is shown in figure 2.7.

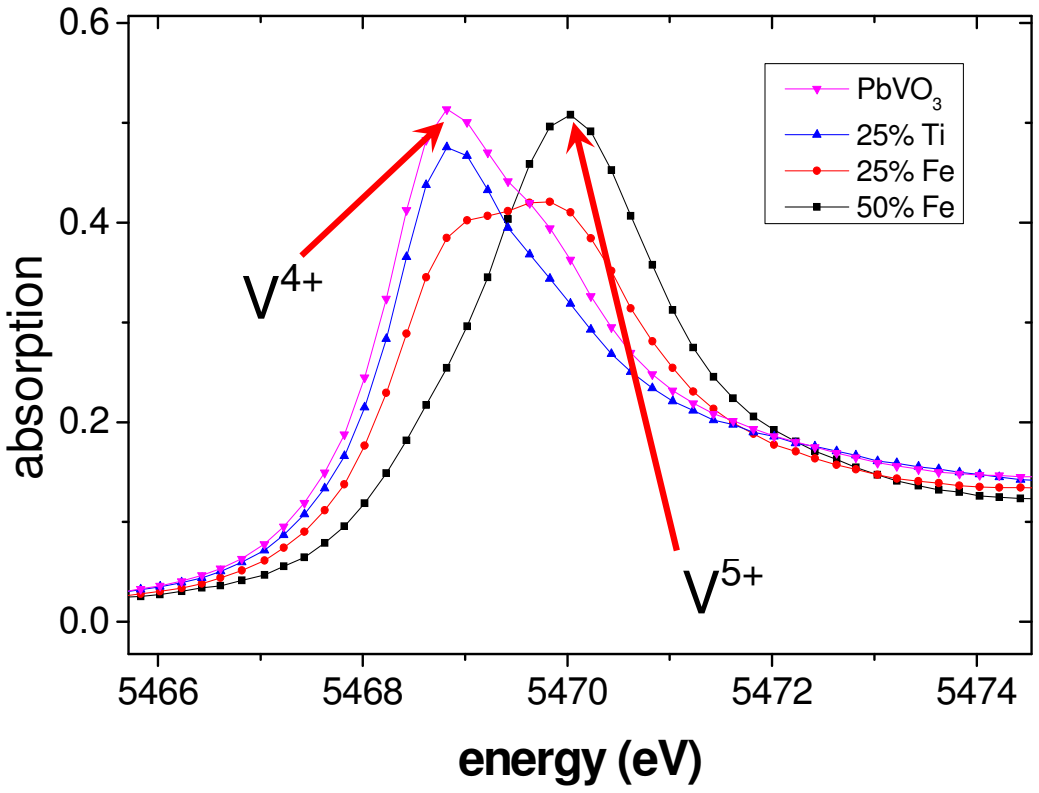

Fig. 2.7. XANES region for XAS of $PbVO_3$, and substitution samples.

The peak on the right corresponds to the 5+ oxidation state and the peak on the left is generated by vanadium oxidized to V^{4+}. It is observed that the position of the peak changes depending on the type and degree of substitution. More specifically a change in

the degree of oxidation of V is observed in the case of the Fe substitution but no such change appears for the Ti substitution.

For $PbVO_3$ (the pink line) the oxidation of V is 4+, as predicted by considering the valence of Pb to be 2+ and that of oxygen 2-. In the case of the Ti substitution, Titanium is also 4+ oxidized so a Ti^{4+} ion replaces a V^{4+} ion and other than that no modification occurs. The peak of the 25% Ti sample (blue line) is at the same energy as the one of $PbVO_3$ meaning that indeed in the Ti series, the Vanadium ions remain 4+. The substitution with Ti is therefore isovalent and this is what allows the formation of the complete solid solution, seen by XRD. The formula of the compounds from the Ti series should in fact be written as $\mathbf{Pb(V^{4+}_{1-x}\,Ti^{4+}_{x})O_3}$.

Iron is generally Fe^{3+}. Fe^{4+} also exists but it is unstable so, it is possible to assume that the iron cations are Fe^{3+}. We also assume that Fe takes the place of V and not Pb so the substitution remains only at the B site cation. In this assumption Fe^{3+} has to replace V^{4+} and this leads to an imbalance of the valence. In order to restore the balance another vanadium ion from the sample increases its oxidation state to 5+ (vanadium will always go to 5+ if it has the opportunity) so the average oxidation state at the B site remains 4+. That means that strictly speaking for every Fe^{3+} ion introduced in the sample two V^{4+} ions are "removed". The first V^{4+} to be removed is the ion directly replaced by Fe^{3+} and the second V^{4+} that is removed is the V^{4+} that oxidizes to V^{5+}. In that case, the formula of the product is $\mathbf{Pb(V^{4+}_{1-2x}\,V^{5+}_{x}\,Fe^{3+}_{x})O_3}$. This explains why the solid solution stops at 50% Fe since at 50% Fe practically all the V^{4+} ions are exhausted. All the vanadium that remains in the 50% Fe sample is vanadium 5+. This can be verified in the peak position of the respective sample (the black line), which shows that the oxidation state of Vanadium is 5+. The sample with 25% Fe is half way into the solid solution and contains both V^{4+} and V^{5+}. The peak of the 25% Fe (red line) has the shape of the convolution of two other peaks (namely the peaks of V^{4+} and V^{5+}) which confirms the presence of both types of vanadium ions in the sample and the validity of the theory.

Chapter III. Crystalline structure from XRD and NPD measurements

III.1. Crystalline structure of $PbVO_3$

$PbVO_3$ is a perovskite oxide, it crystallises in a tetragonal structure with the space group P4mm and the lattice parameters a ≈ 3.8 Å and c ≈ 4.67 Å. The Pb atoms occupy the 1a (000) position at the corners of the unit cell and the V atoms are located at the 1b (1/2 12/ z~0.57) position strongly displaced from the centre of the cell along the c axis. The oxygen atoms are also largely displaced from the face centres they would occupy in the archetypal cubic perovskite structure with O1 at 1b (1/2 1/2 z~0.22) and O2 at 2c (1/2 0 z~0.69). They form a strongly elongated octahedron which is shifted from the unit cell centre along the c axis. As a result, the vanadium coordination can be considered as square pyramidal with a quite short V-O1 distance (1.65 Å) and four longer V-O2 distances (1.98 Å). Figure 3.1 shows a representation of the structure of $PbVO_3$.

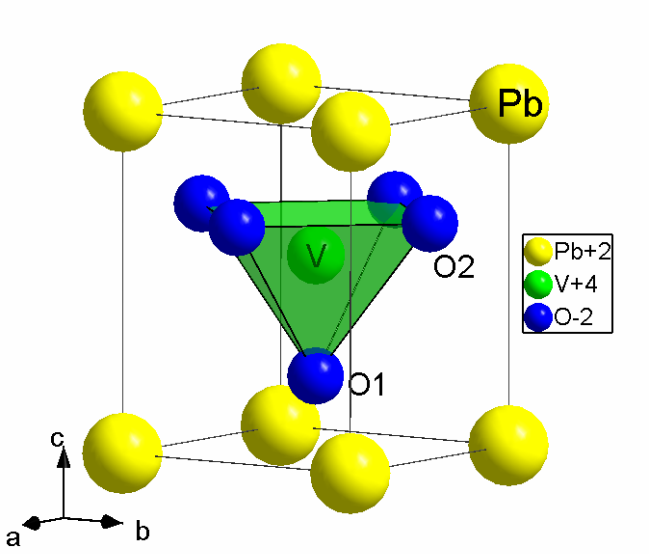

Fig. 3.1. Structure of $PbVO_3$.

This structure was refined for the first time using the data collected from single crystal X-Ray diffraction measurements. The X-Ray diffraction data were collected using a Bruker Kappa ApexII diffractometer with a silver anode, AgKα, λ = 0.56087. The gof (goodness of fit) of the refinement was 1.6. The lattice parameters found are a=3.798(3) Å respectively c=4.662(11) Å, in good agreement with data available in literature (from powder diffraction). The interatomic distances and anisotropic atomic displacements parameters are determined to a much better precision and accuracy from single crystal diffraction data than from powder diffraction data. The

non-centro symmetric nature of the structure is unambiguously confirmed, so as the ferroelectric nature of the compound which is also supported by the presence of ferroelectric twin domains. Table 3.1 gives the atom positions and the atomic displacement parameters obtained from the refinement.

Table 3.1. Atomic positions and displacement parameters obtained from the refinement of single crystal diffraction data.

a) Positional parameters

Atom	Wyckoff	x	y	z	Ueq (Å^2)
Pb	1a	0	0	0	0.01008(5)
V	1b	0.5	0.5	0.5690(3)	0.0089(2)
O1	1b	0.5	0.5	0.215(2)	0.0145(14)
O2	2c	0.5	0	0.6900(14)	0.0120(11)

b) ADP harmonic parameters (Å^2)

Atom	U_{11}	U_{22}	U_{33}	U_{12}	U_{13}	U_{23}
Pb	0.00828(8)	0.00828(8)	0.01368(11)	0	0	0
V	0.0067(3)	0.0067(3)	0.0133(5)	0	0	0
O1	0.014(2)	0.014(2)	0.015(3)	0	0	0
O2	0.010(2)	0.0093(19)	0.017(2)	0	0	0

III.2. Crystallographic data for the substitution series

All the samples, regardless of the substitution, were measured using XRD in a D 5000 diffractometer, equipped with a Cu anode, in transmission geometry, in the angle range of 10-90° (2θ) with a step of 0.016° and 10 seconds counting time for every step. Again, the difractograms were refined using the Rietveld method with the FullProf software.

A standard sample of LaB_6 was measured at the same device in the same conditions. This allowed the determinations of the instrumental contribution to the peak broadening and made possible the measurement of the sample's grain size and mechanic strain.

III.2.1. Ti series lattice parameters

Figure 3.2 shows the XRD patters for the Ti substituted samples at 0, 25, 50, 75 and 100 % substitution.

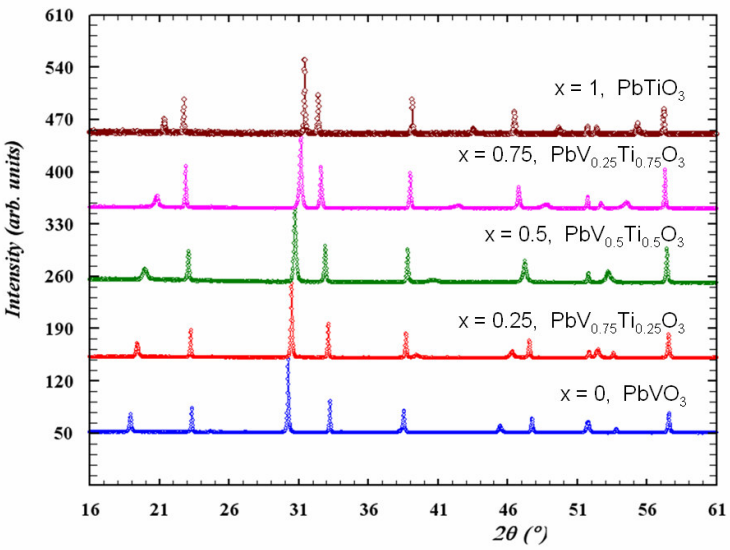

Fig. 3.2. XRD patterns obtained for 5 representative samples from the $PbV_{1-x}Ti_xO_3$ series, namely the samples for x = 0, 0.25, 0.5, 0.75 and 1.

For the Ti series we observed a linear change in lattice parameters with the degree of substitution. A solid solution thus exists in between $PbVO_3$ and $PbTiO_3$. The variation of lattice parameters in function of the Ti concentration is presented in figure 3.3.

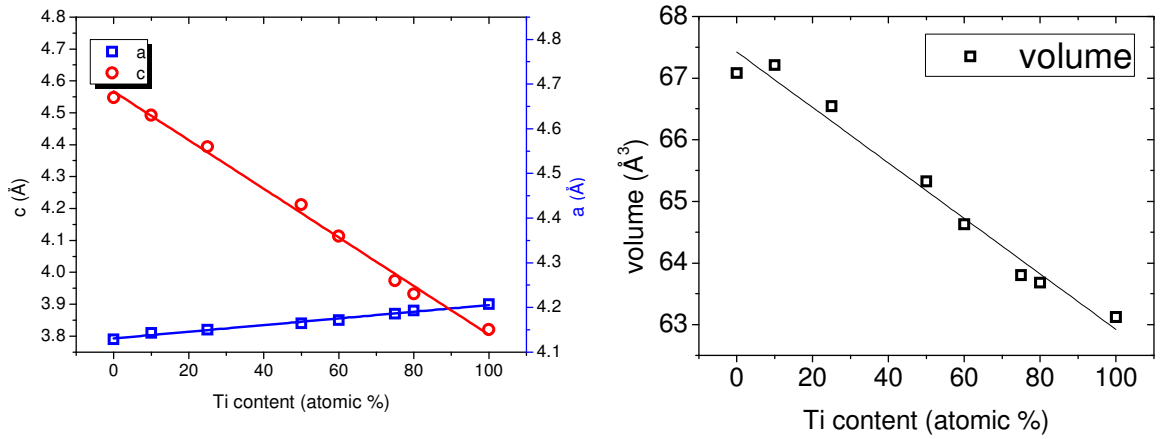

Fig. 3.3. Modification of the lattice parameters (left) and evolution of the cell volume (right) vs. nominal degree of substitution, x, in $Pb(V_{1-x}Ti_x)O_3$. Linear fits are drawn to guide the eyes.

III.2.2. Ti series microstructure

The width of reflections shows a clear evolution with respect to substitution ratio. The broadening of peaks from sample effects is known to originate from two types of physical data: the grain size and the presence of local strain. We had observed that reflections that were close to the c* axis were systematically broader. The model employed to describe this anisotropy had two components:

- an uniaxial lorentzian size parameter controlling the size effects,
- five parameters (S400, S004, S220 and S202 plus a lorentzian strain coefficient) describing strain effects, using the formulation of Stephens [25].

The grain size has a minimum at about 50% Ti substitution, the half way between $PbVO_3$ and $PbTiO_3$ (figure 3.4 a). Strain for the same Ti series, follows an almost constant variation with the composition, as seen in figure 3.4 b.

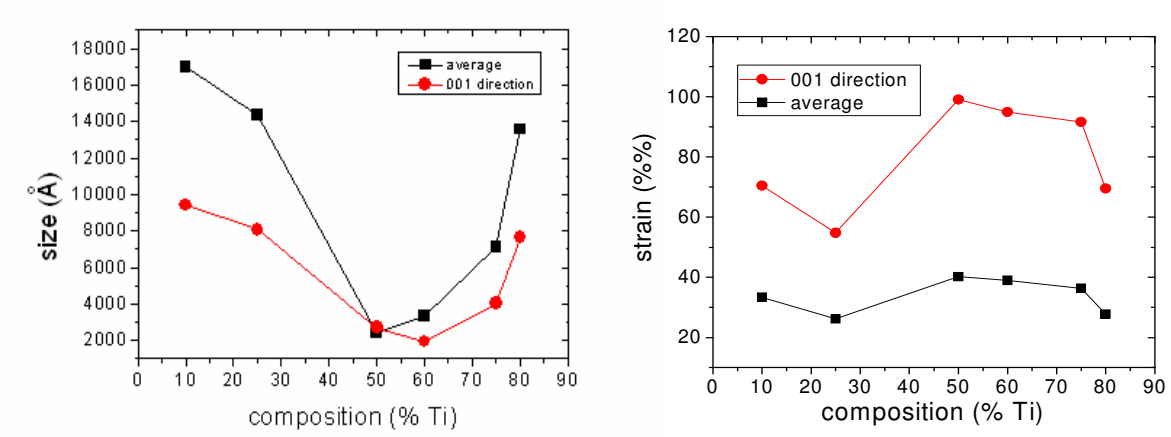

a) b)

Fig. 3.4. Variation of a) grain size and b) stain with the composition for the Ti series. Red points represent values along the c axis and black points represent average values*

III.2.3. Ti series structure

From XRD refinements small modifications in the atom coordinates were observed as the content of Ti is increased. The z for the B site cation decreases from z = 0.564(2) for the 10% Ti sample to z = 0.545(1) for the 80% Ti sample. It seems the B site cation

tends to go towards the centre of the unit cell (at z = 0.5), the apical oxygen moves towards the face of the unit cell (z = 0) and the other oxygen anions try to go to face centres (z = 0.5) as if the system begins to transform in a cubic structure. This is consistent with a decrease of the ferroelectric distortion upon V substitution for Ti, which is expected since $PbTiO_3$ is known to be less distorted than $PbVO_3$.

III.2.4. Fe series lattice parameters

Figure 3.5 shows the XRD patters for the Fe substituted samples at 0, 10, 20, 30 and 40 % substitution.

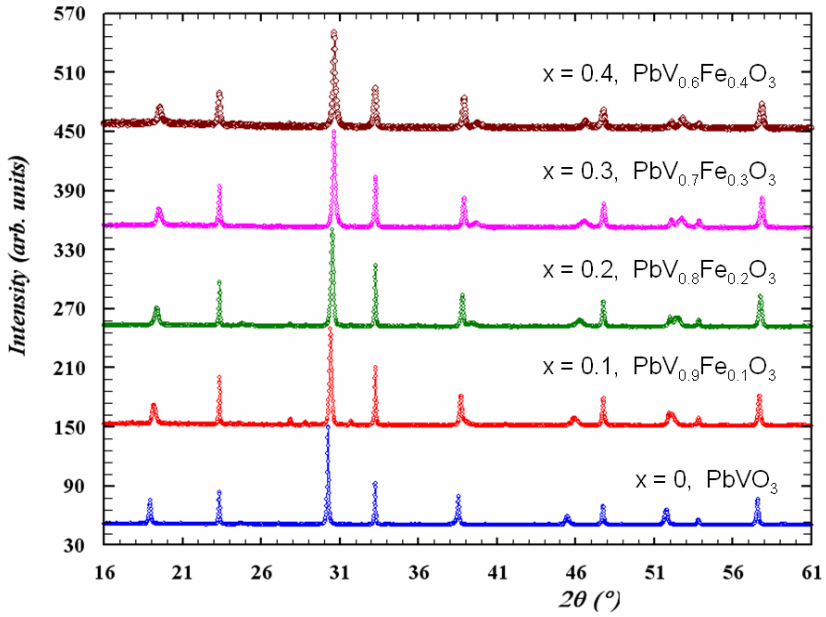

Fig. 3.5. XRD patterns of representative samples of the Fe substitution compounds, $PbV_{1-x}Fe_xO_3$, where x = 0, 0.1, 0.2, 0.3 and 0.4.

For the Fe series the solid solution stops at x = 0.5. The tetragonal structure is conserved for x < 0.5. At x = 0.5 a new phase with cubic symmetry appears and a mixture of the two phases is observed. For x > 0.5 the tetragonal phase vanishes. In the tetragonal phase, the increase of iron percentage decreases the c parameter but does not change a.

The variation of lattice parameters and the leap to a new cubic phase are represented in figure 3.6.

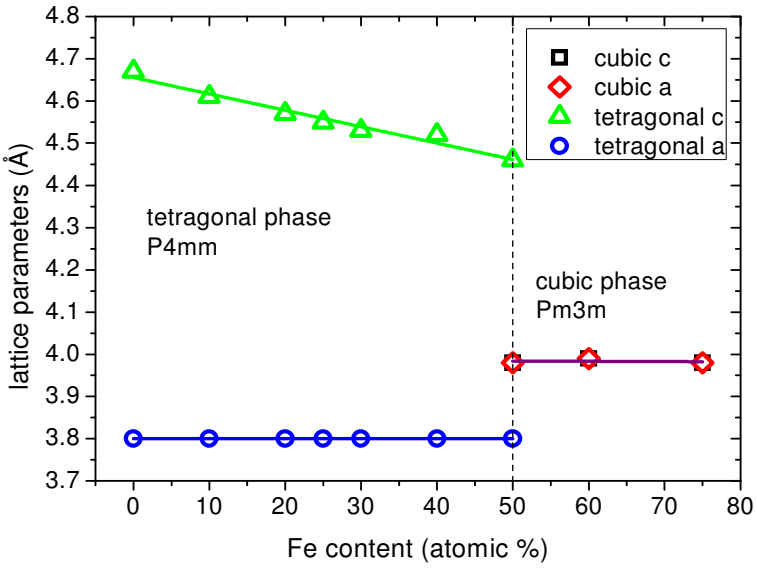

Fig. 3.6. Variation of lattice parameters and phase transition for $Pb(V_{1-x}Fe_x)O_3$.

III.2.5. Fe series microstructure

The results obtained for the Fe series are presented in figures 3.7 a and b. It can be observed in the graph that the average grain size is greater than the grain size on the c axis. That means that the grains, the crystallites, are shorter on the c direction and have a flat aspect.

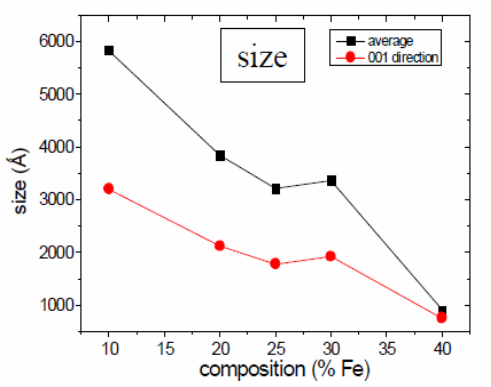

a)

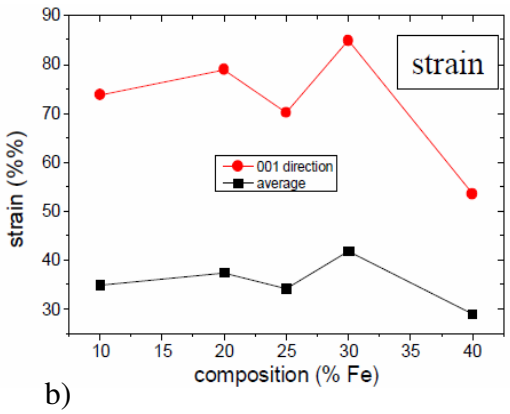

b)

Fig. 3.7. Variation of a) grain size and b) stain with the composition for the Fe series. Red points represent values measured along the c axis and black points represent average values.*

The strain does not vary significantly with the composition but remains nevertheless much larger along the (0 0 1) direction than the average value, indicating a strongly anisotropic strain with c as the preferred axis.

As a conclusion to this study of the microstructure of substituted samples, we have shown that substitution at the V site generates planar defects which can be interpreted as ferroelectric antiphase domains oriented perpendicular to the c axis. The disorder introduced by substitution decreases the coherent domain size, more efficiently for Fe than for Ti substitution, without additional change of the structural global strain.

III.2.6. Fe series structure

Again some small variations in atomic positions are seen and these variations appear to show the system slightly shifting towards a cubic structure. Fe does not form an equivalent to the short strong vanadyl bond so the average V/Fe-O1 distance increases slightly. We observed little change in the vanadium coordination, and a tendency for the Fe cations to adopt a less distorted coordination, with longer Fe-O1 bonds. When the amount of iron is increased, the quality of refinement becomes somewhat poorer. Contrarily to the case of titanium, the substitution is no longer isovalent for Fe and the B cation site of the perovskite is now occupied by V^{4+}, V^{5+} and Fe^{3+}, each with its own coordination sphere.

III.3. Raman investigations

The local structure of the samples was investigated by Raman spectroscopy. The data were collected for four representative samples, namely $PbVO_3$, and tree substitution samples: 25% Ti, 25% Fe and 40% Fe. Figure 3.8 shows the superposition of the Raman spectra for these samples.

It can be observed that the most active vibrations are those that appear at high wavenumbers (about 800 cm^{-1}) which are identified as $A_1(3TO)$ respectively $A_1(3LO)$

and belong to the B site cation - apical oxygen stretching. Their evolution is marked by line (1). Line (2) marks the evolution of the A_1(2TO) and by extension A_1(2LO) modes, associated to the bending of the O-B cation-O bond.

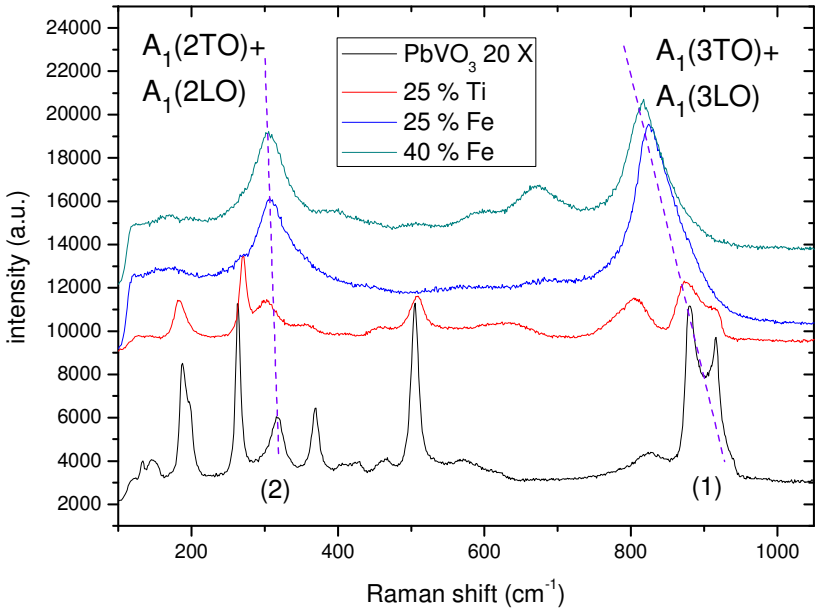

Fig. 3.8. Superposition of the Raman spectra for all 4 samples. Two lines are plotted for eye guidance and to indicate the evolution of the vibration modes considered.

The vibration modes observed for $PbVO_3$ can be identified by comparison to data available for $PbTiO_3$ bulk samples and $PbVO_3$ thin films. The 25% Ti sample presents the A_1(3TO) and A_1(3LO) modes which can be attributed separately to the Ti-O1 and to the V-O1 stretching vibrations. It might be inferred that the V-O1 bond is shorter and stronger than the Ti-O1 bond (where O1 denotes the apical oxygen) since it appears at higher wavenumbers. This result is consistent with observations based on diffraction experiments. For the iron substitution samples there is a convolution of the A_1(3TO) and A_1(3LO) which generates a single broad peak cantered at about 842 cm^{-1}. The widening of the peak could be explained by the fact that the sample contains 3 different cations at the same crystallographic place (V^{4+}, V^{5+}, Fe^{3+}), each cation forming a different bond hence generating a different peak at a slightly different wavenumber. What is observed is the convolution of those peaks. The peaks at high wavenumbers (about 800 cm^{-1}) are displaced towards lower wavenumbers as the substitution degree increases. This suggests the weakening of the average B site cation - apical oxygen bond and is clearly observed between the samples containing 25% Fe and 40% Fe. This effect is consistent with results obtained from XRD / NPD experiments.

Chapter IV. Magnetic characterization

IV.1. Magnetic properties of $PbVO_3$

Magnetic measurements were conducted in a SQUID type magnetometer, in the temperature range of 2 to 350 K and in magnetic fields ranging from 100 Oe to 5 Tesla.

The magnetic susceptibility in function of temperature for $PbVO_3$ was measured between 2 K and 350 K. The $\chi(T)$ graph for $PbVO_3$ is shown in figure 4.1. The general shape of the curve is similar to what has been reported in literature [16,17]. The features of the curve are a broad peak at about 180 K and an upturn of the susceptibility at low temperatures ($T < 50$ K). The magnetic signal of $PbVO_3$ is very small. The small value of this signal and the shape of the $\chi(T)$ curve are explained in literature by 2D AFM models. We tested two models, namely the Heisenberg square lattice model (SQL) and the frustrated square lattice model (FSL) and observed that both describe reasonably well the behaviour of the susceptibility in the high temperature region (200K – 300K, see figure 4.1).

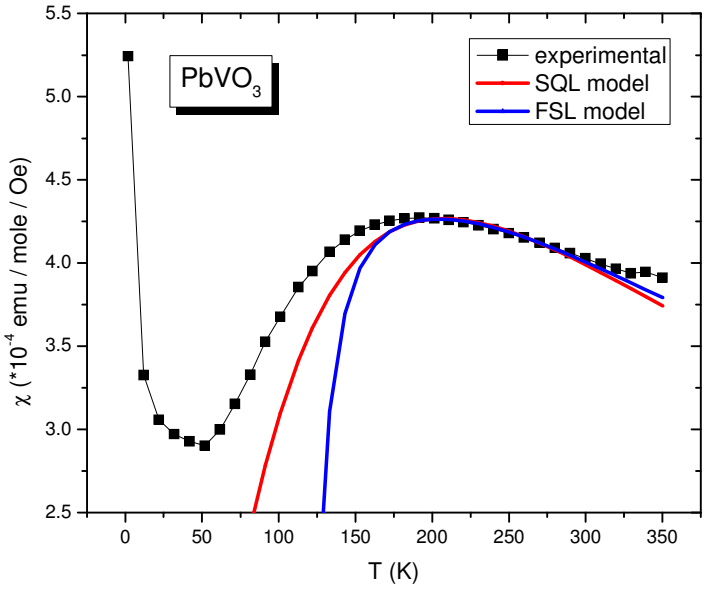

Fig. 4.1. $\chi(T)$ for $PbVO_3$, SQL and FSL fits for the $\chi(T)$ data. Black points represent the experimental $\chi(T)$. The SQL fit is shown by the red line and FSL fit is the blue line.

The SQL model assumes the formation of a long range 2D antiferromagnetic lattice. The magnetic susceptibility for this case is described by the subsequent equation [17]:

$$\chi(T)=\frac{Ng^2{\mu_B}^2}{4k_BT}\left[1+\left(\frac{J}{k_BT}\right)+\frac{1}{2}\left(\frac{J}{k_BT}\right)^2+\frac{1}{6}\left(\frac{J}{k_BT}\right)^3+\frac{1}{64}\left(\frac{J}{k_BT}\right)^4\right]^{-1}+\chi_0$$

,where J is the exchange integral and χ_0 is a diamagnetic component.

The FSL model considers the formation of a frustrated 2D antiferromagnetic structure by also taking into account the interactions with the next nearest neighbour. The susceptibility for this case is described by the following equation [26]:

$$T\chi=\sum_n \beta_1^n \sum_m c_{m,n}x^m$$

Both models returned a value for the exchange interaction of about 218 K.

The formation of the 2D lattice is connected to the formation of the vanadyl bond between the V^{4+} cation and the apical oxygen. The V cations are connected by a super-exchange interaction through the oxygen anion. The nature of this interaction is strongly dependent on the V-O distances. The V^{4+} cation is surrounded by an oxygen octahedron but it is shifted from the centre of the octahedron by the strong vanadyl bond. The in plane distance (V-O2) is 1.98 Å. The short out of plane distance is 1.64 Å to the apical oxygen (V-O1) but the out of plane distance towards the other oxygen anion is 3.03 Å. This large distance prevents the formation of the super-exchange interaction perpendicular to the (a,b) plane therefore correlations of the V cations are confined to the 2D system. On the other hand it has been shown by Uratani [27] that the 1d electron of V occupies the d_{xy} orbital which is parallel to the V-O_2 layers this constituting a second reason for which the system is expected to be two dimensional.

IV.2. Magnetic properties of the Ti substitution series

When the vanadium from $PbVO_3$ was substituted by titanium it was observed that the system becomes paramagnetic and the magnetism of $PbVO_3$ becomes progressively diluted. Figure 4.2 shows a zoom on the curves of the magnetic susceptibility of 3 samples from the Ti series, namely $PbVO_3$, $PbV_{0.9}Ti_{0.1}O_3$ (10% Ti) and $PbV_{0.5}Ti_{0.5}O_3$ (50% Ti). The susceptibility of the latter presents an increase of value with the decreasing temperature which is typical for a paramagnet (figure 4.2b shows the entire susceptibility curve for the 50% Ti sample).

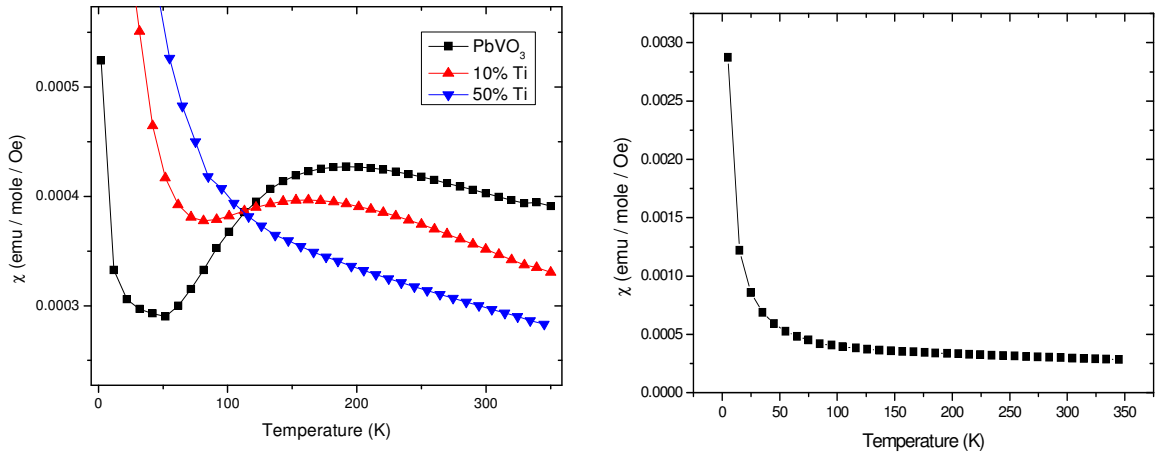

Fig. 4.2. a) χ(T) for $PbVO_3$ sample and for the samples containing the 10% Ti and 50% Ti substitutions. A broad peak can be observed on the susceptibility of the 10% Ti sample, while the same peak disappears for the 50% Ti sample, b) entire χ(T) curve for $PbV_{0.5}Ti_{0.5}O_3$.

The sample with 10% Ti is interesting because it still presents the very broad peak in susceptibility of $PbVO_3$, centred at about 170 K, which marks the presence of 2D AFM correlations, but it also shows an increase of the susceptibility with the decreasing temperature, which defines a paramagnet. This places the sample between the magnetic behaviour of $PbVO_3$ and the paramagnetism of the samples with higher degrees of substitution and highlights the dilution of the magnetism of the parent compound, $PbVO_3$. The same effect is observed from the reduction of the overall magnetic moment with the

increase of the substitution (figure 4.3). The experimental moment is calculated from the slope of the $1/\chi(T)$ plot. This moment is compared with the estimated theoretic moment, assuming a magnetic moment of $\mu = 1.73\ \mu_B$ for the vanadium ions.

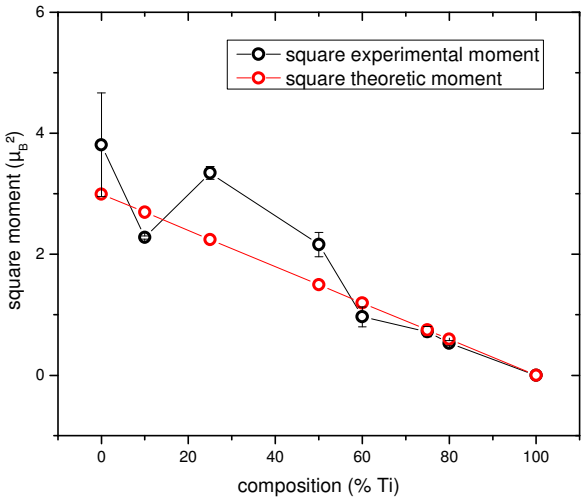

Fig. 4.3. Observed and calculated effective moments for the samples in the Ti series.

IV.3. Magnetic properties of the Fe substitution series

In the case of the iron substitution a magnetic transition is visible in the samples in the difference between zero field cooled (ZFC) and field cooled (FC) measurements (see figure 4.4).

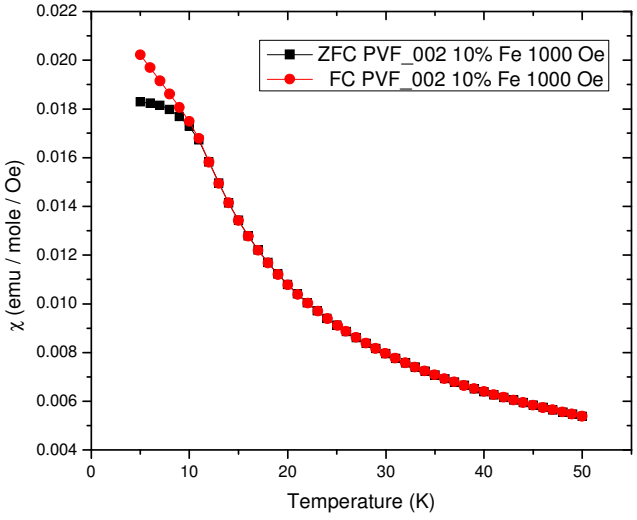

Fig. 4.4. ZFC-FC split for $PbV_{0.9}Fe_{0.1}O_3$.

In the M(H) measurements a magnetic hysteresis is observed at low temperatures (2K). This indicates the presence of ferromagnetic interactions, even though the hysteresis is very narrow, see figure 4.5.

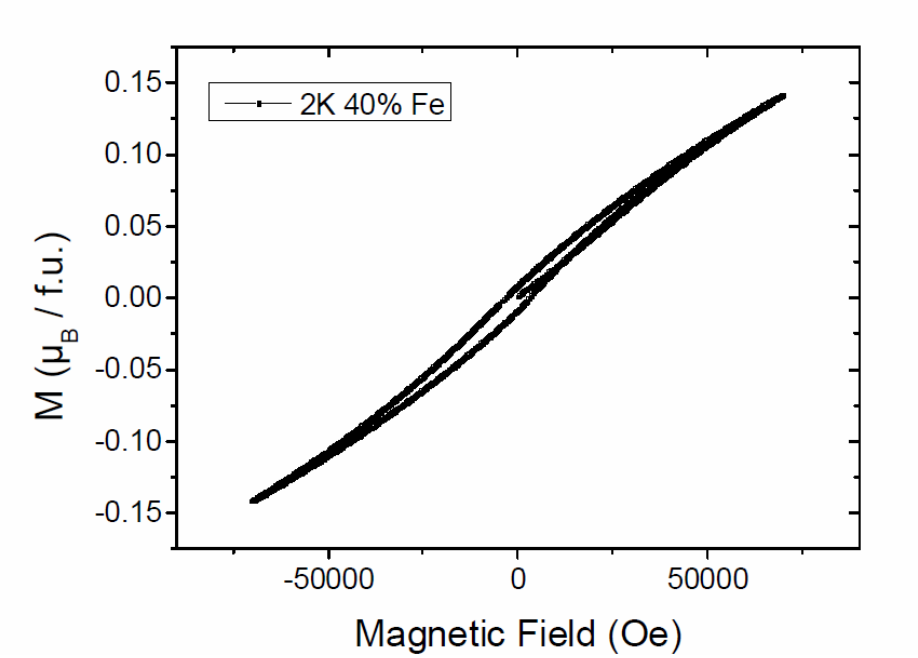

Fig. 4.5. Magnetic hysteresis for $PbV_{0.6}Fe_{0.4}O_3$. Notice in the centre of the curve the difference between the first magnetization path and the return to zero field path.

All the iron doped samples present the ZFC-FC splitting. The temperature of the magnetic transition (identified from the $\chi(T)$ curves) increases with the iron concentration, see figures 4.6 and 4.7. For clarity only 5 samples are selected for showing the presence of a magnetic transition in the Fe series. The representation is stopped at 40% Fe substitution because that is the last step before reaching the cubic phase, as discussed in the previous chapter. Figure 4.6 shows the ZFC curves for representative samples from the Fe series.

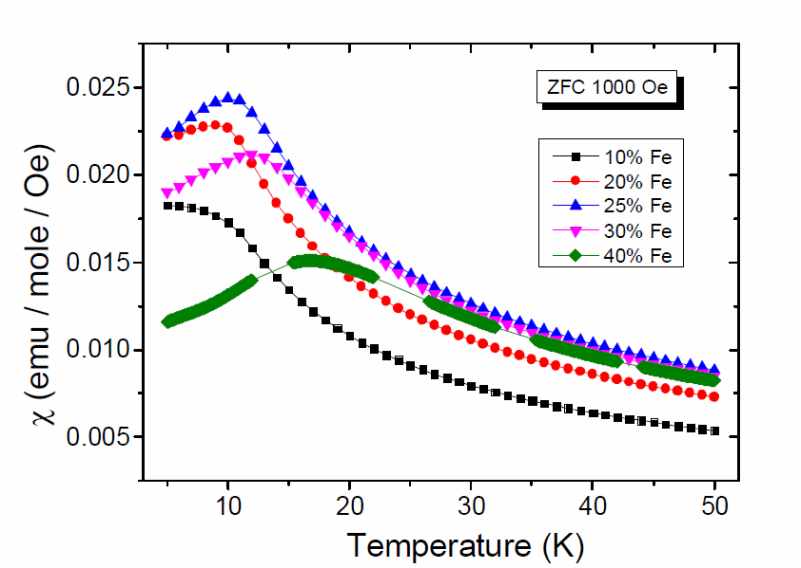

Fig. 4.6. Magnetic transition in iron doped samples.

Figure 4.7 shows the increase of the χ(T) transition temperature with the Fe content. The value for the transition temperature is calculated from the first derivative of the χ(T) curve.

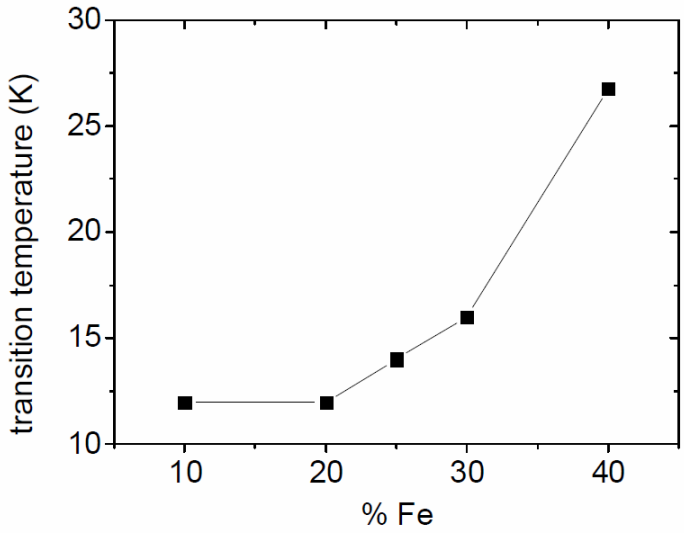

Fig. 4.7. The variation of the transition temperature in function of composition.

On the same samples, the plot of the inverse susceptibility in function of temperature indicates the presence of antiferromagnetic interactions. This is observed from the fact that the extension of the linear region of the plot intersects the x axis in the

domain of negative temperatures. Figure 4.8 shows the plot of the inverse susceptibility in function of temperature for the samples discussed above.

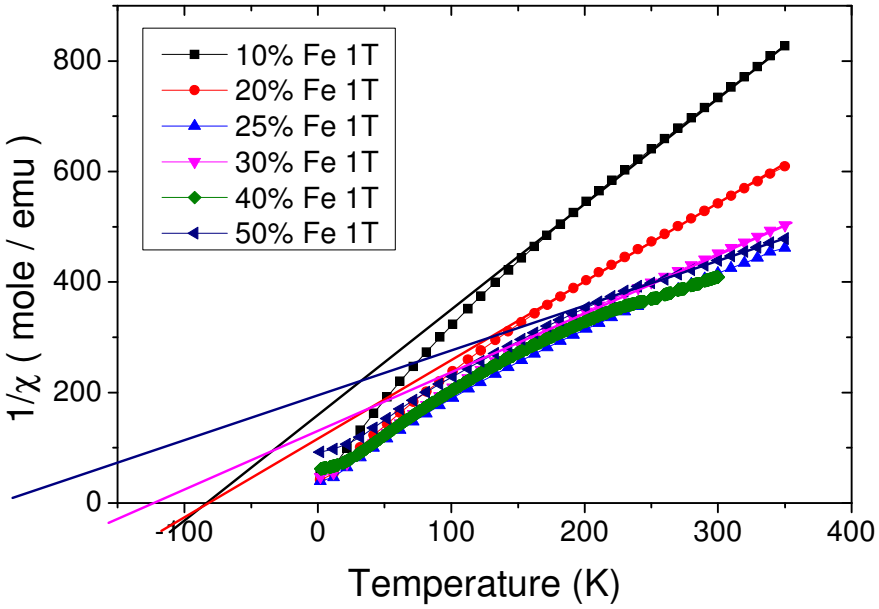

Fig. 4.8. 1/χ vs T plot for the Fe series. Lines extended from linear regions of the 1/χ graphs are traced and found to intersect the temperature axis in negative side.

The effective magnetic moment was calculated from the slope of the 1/χ plot for all the sample of the $PbV_{1-x}Fe_xO_3$ system for which $x \leq 0.5$. The calculation was performed on the high temperature domain (200 - 300 K).

The magnetic moment per unit cell obtained from the fit shows the tendency to increase as more iron is introduced into the sample and varies linearly with the composition. The theoretic effective moment was found to approach the experimental values when it is calculated assuming the moments for the V^{4+} and for Fe^{3+} as $\mu_V = 1.73$ μ_B and $\mu_{Fe} = 4.79$ μ_B respectively and considering that each Fe^{3+} ion introduced in the sample replaces two V^{4+} ions (see the XAS results).

Figure 4.9 shows the evolution of the magnetic moment with the iron content.

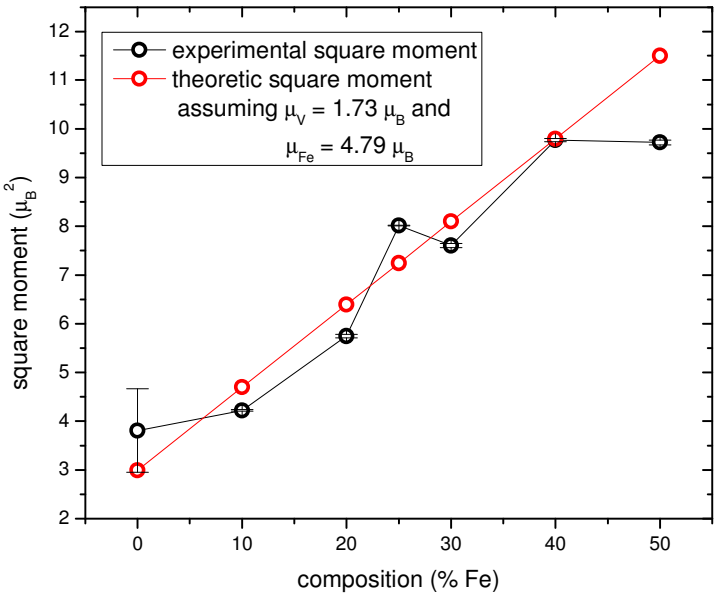

Fig. 4.9. Magnetic moment in function of composition, calculated from the Curie Weiss law fit of the experimental data.

The magnetic moment of the Fe^{3+} cation is expected to be $\mu_{Fe} = 5.92\ \mu_B$ assuming the relation for the spin only contribution $\mu_{eff} = g\sqrt{S(S+1)}$ for S = 5/2. However better results are obtained assuming a magnetic moment of the Fe cation of only $\mu_{Fe} \approx 4.8\ \mu_B$ instead of the expected 5.92 μ_B. The reason for this discrepancy could reside in the fact that the Curie-Weiss fit was performed in a region that was not far enough from the transition temperature so the sample did not had a purely paramagnetic behaviour yet and some antiferromagnetic correlations of the Fe^{3+} moments were still present. Their presence could be responsible for the decrease of the magnetic moment of the Fe^{3+} cation.

IV.4. Testing for spin glass behaviour

The type of magnetic structure was investigated by neutron powder diffraction (NPD). However, NPD patterns revealed neither extra magnetic peaks nor any change of intensity at the crystallographic peaks when the system was cooled below the temperature of the magnetic transition detected by susceptibility measurements. Specific heat measurements on the same temperature range also revealed no transition. These results could indicate the absence of any long range ordering. Short range ordering could exist

however, leading to the formation of a spin glass system. This scenario is supported by a.c. susceptibility measurements. The real part of the susceptibility presents a maximum and that maximum is shifted to higher temperatures with the increase of the frequency (see figure 4.10). This behaviour is characteristic for a spin glass or cluster glass system.

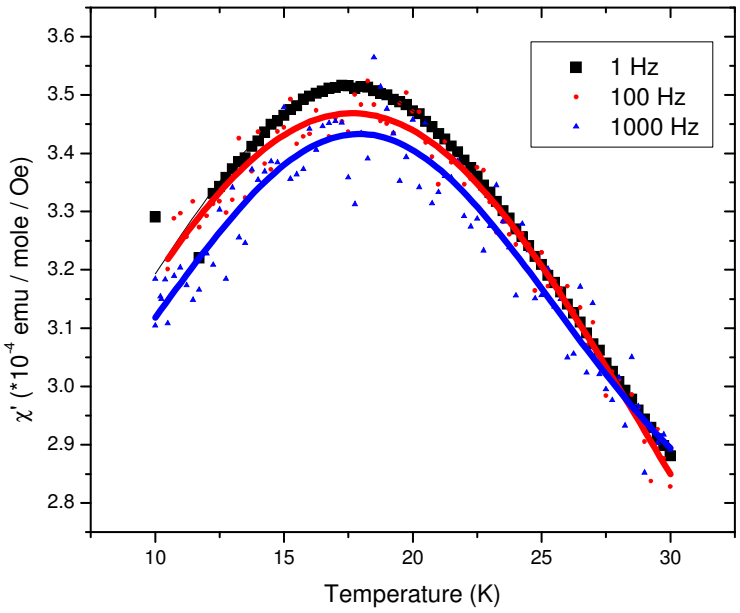

Fig. 4.10. χ'(T) for $PbV_{0.6}Fe_{0.4}O_3$ collected at 3 different frequencies. The signal is affected by electronic noise at higher frequencies so for these measurements Gaussian fit curves are drawn to guide the eyes.

IV.5. Study of local magnetic interactions by EPR spectroscopy

EPR measurements were performed on the same four representative samples ($PbVO_3$, 25%Ti, 25%Fe and 40% Fe). The data were collected from RT to 110 K.

For $PbVO_3$ the EPR results in function of temperature are consistent with the presence of V^{4+} paramagnetic ions in a square–pyramidal C_{4v} coordination (with hyperfine coupling constants $A_{\parallel}$ and $A_{\perp}$). The evolution of the hyperfine coupling constants function of temperature is in agreement with the small increase of unit cell height c with increase of the temperature. This result was also obtained from XRD.

For the 25% Ti sample a sharp variation of the EPR parameters with the temperature is observed. This variation is consistent with the presence of short range magnetic order, confined to distinct spatial regions. Also, the variation is consistent with magnetic susceptibility results.

For the iron substitution samples the resonance spectra exhibit a broad line, centred on g=2 due to the spin of the Fe^{3+} ions. For the 25% Fe sample, an additional resonance mode situated around g=4.2 was evidenced. It is attributed of the presence of Fe^{3+} ions on a tetrahedral environment with a strong rhombic distortion. For the 40% Fe sample a hyperfine structure is observed, overlapping the absorption spectrum of the Fe^{3+} ions. This hyperfine structure is attributed to the presence of V^{4+} ions. The EPR line intensity was observed to decrease with the temperature. The decrease of EPR line intensity suggests the increase of the number of antiferromagnetic pairs Fe^{3+}-Fe^{3+}.

Figure 4.11 shows the EPR spectra for the samples discussed above.

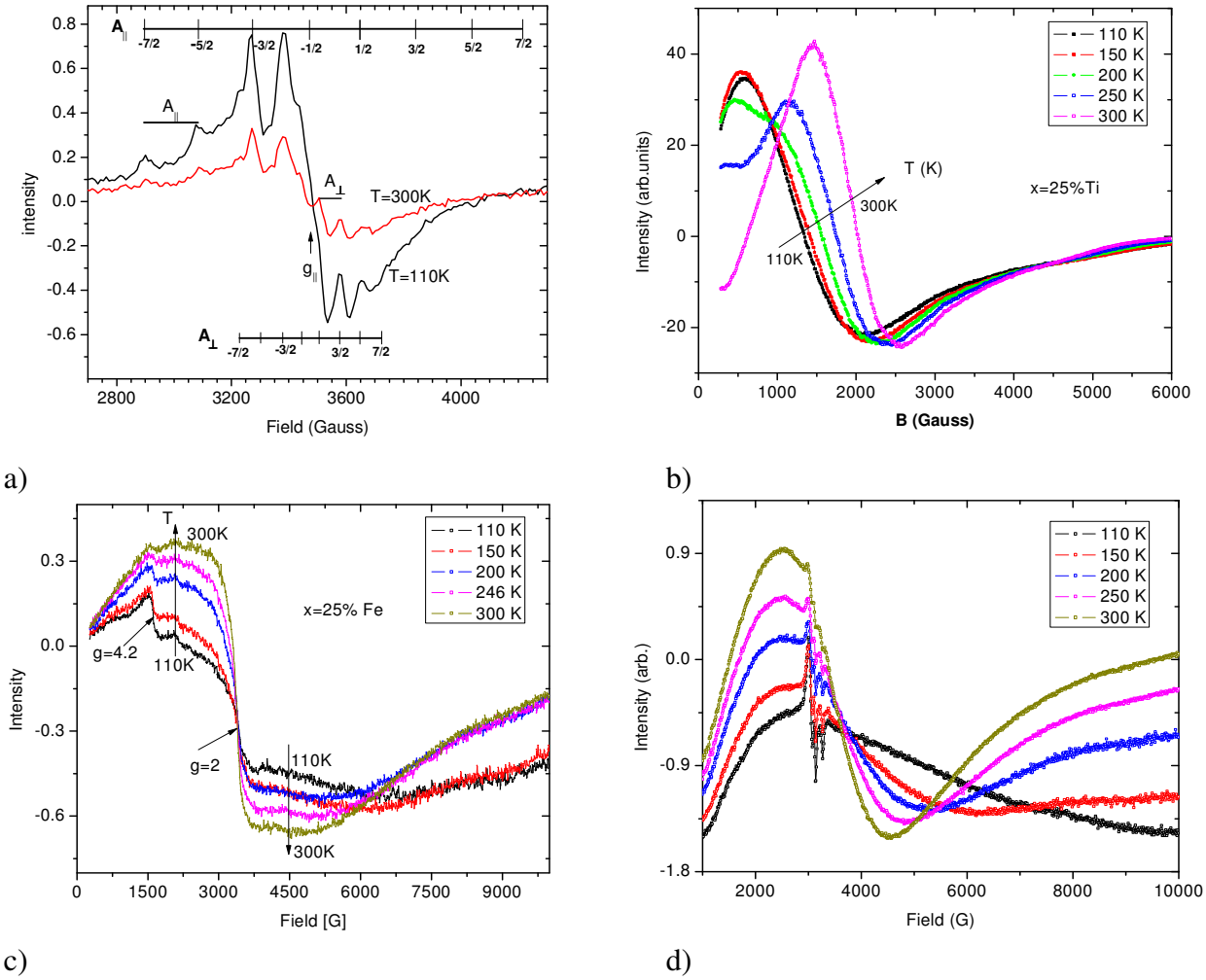

Fig. 4.11. EPR spectra for $PbVO_3$ (a), 25% Ti (b), 25% Fe(c) and 40% Fe (d).

IV.6. Electrical resistivity, dielectric constant and polarization

Electrical resistivity was measured by the 2 contacts method on $PbVO_3$ single crystals. Measurements of dielectric constant, ε_r, were performed on a small piece of sintered powder with the composition containing 40% Fe ($PbV_{0.6}Fe_{0.4}O_3$). The impedance of the sample is measured and the sample is modelled with a parallel RC circuit. The capacitance of the sample is returned by the impedance meter. Polarization measurements were attempted on a $PbVO_3$ single crystal using a Sawyer-Tower circuit.

The ρ(T) measurement revealed a semiconductor behaviour with the resistivity increasing exponentially with the decrease of temperature. Figure 4.12 shows the ρ(T) graph (a) and the logarithmic plot of the resistivity measurement (b).

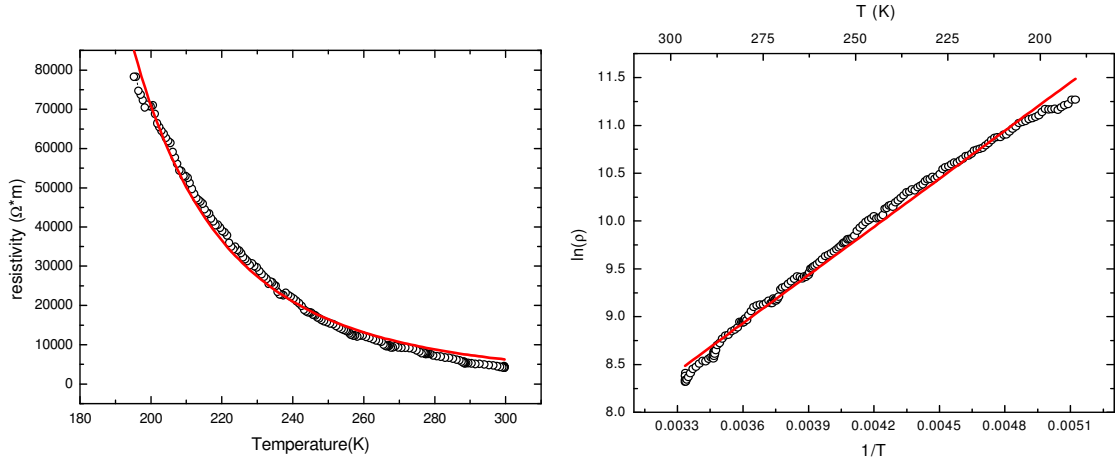

a) b)

Fig. 4.12. a) ρ(T) for $PbVO_3$, b) ln(ρ(T)) for the same sample. The dots represent the experimental points and the lines represent the corresponding fits.

The value of the gap energy calculated from these plots is estimated at Eg = 0.25(1) eV for the ρ(T) fit and Eg = 0.28(8) eV from the logarithmic plot.

Dielectric constant measurements were performed for the $PbV_{0.6}Fe_{0.4}O_3$ sample. Figure 4.13 shows the variations of the dielectric constant of the sample and the tanδ with the temperature for 3 different frequencies.

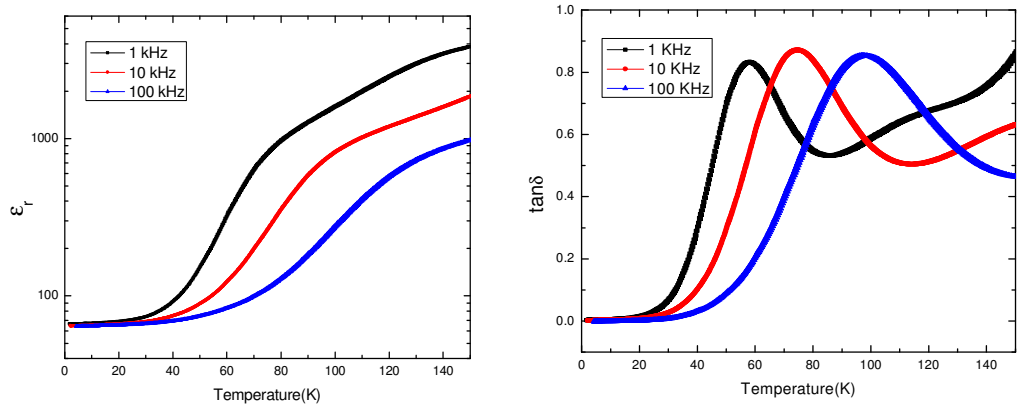

a) b)

Fig. 4.13. a) Variation of the dielectric constant ε_r with the temperature for the 40% Fe sample, b) variation of tanδ with the temperature for the same sample. These measurements were conducted at the frequencies of 1 kHz, 10 kHz and 100 kHz respectively.

A board peak can be observed in the graph of tanδ and the position of the peak shift towards higher temperatures as the frequency of the measure is increased. This is a typical behaviour of a ferroelectric relaxor. By contrast, for a normal ferroelectric the tanδ presents a sharp peak at a temperature that is independent of the frequency measurement [28, 29]. Relaxor ferroelectrics are the equivalents of the magnetic spin glasses. Cross [29] proposed a model which explains the frequency response of the ferroelectric relaxors. The model supposes that the small size of the polar domains of a relaxor (several tens of nanometres) causes these domains to behave like superparaelectric domains by equivalence to the superparamagnetic domains from magnetism. Each domain has its own return frequency f_R. The frequency dependence becomes:

$f_R = f_0 * \exp(-E_A/K_BT)$ where E_A is the activation energy.

For the 40% Fe sample the values for the activation energy and relaxation time were $E_A = 0.0522(1)$ eV and $\tau_0 \approx 2.89*10^{-8}$ s which is consistent with the values expected for a ferroelectric relaxor (E_A between 0.05 and 0.075 eV and τ_0 between $5*10^{-13}$ and $7*10^{-6}$ s) [30].

The transformation of the system from a true ferroelectric material ($PbVO_3$) to a ferroelectric relaxor with the substitution of vanadium with iron can be explained by the disordered induced as a result of the substitution. The perovskite relaxors are almost always disordered crystals which contain some substitution (isolavent or not) at the B site cation. Also the presence of mixed valence states appears to favour the formation of a relaxor ferroelectric. $Pb(V_{1-x}Fe_x)O_3$ (for $x<0.5$) contains 3 different cations at the B site, namely V^{4+}, V^{5+} and Fe^{3+} all presenting close ionic radii (0.53 Å for V^{4+}, 0.46 Å for V^{5+}, 0.58 Å for Fe^{3+}). The small differences of ionic radii could favour a random distribution of the cations which tends to reduce the tendency for long range ordering, possibly by a similar phenomenon as the one observed on Sr_2FeTiO_6 [30]. SEM images reveal the presence of ferroelectric domains (in the Fe substitution samples) which are limited to a few tens of nanometres. This is another characteristic of ferroelectric relaxors.

Polarization measurements were attempted on a $PbVO_3$ single crystal. The result is shown in figure 4.14. The circuit was driven by a step up transformer that could output a voltage of about 1000 V. The length of the crystal was approximately 500 μm so the order of magnitude of the electric field applied had an intensity of about 2.10^6 V/m, far below the predicted 1.10^9 V/m field supposedly required to reach the saturation of the sample.

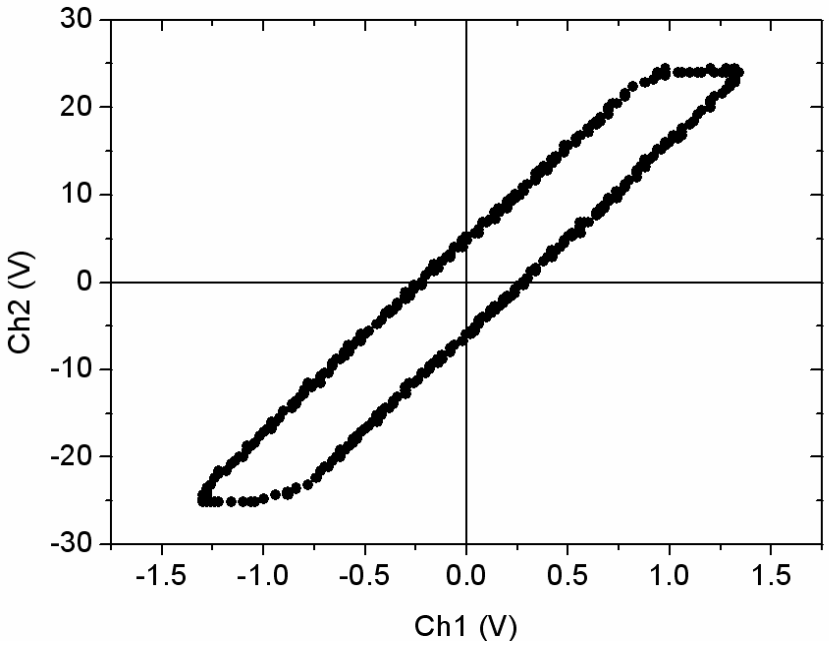

Fig. 4.14. Polarization hysteresis for $PbVO_3$. The measurement is made at RT with a frequency of the applied AC signal of 150 Hz.

On the above figure Ch1 (channel 1) is the voltage measured on the contacts to the sample and Ch2 is the voltage measured across the reference capacitor.

A hysteresis in the polarization can be observed. However the value of saturation polarization of $PbVO_3$ could not be reached and reasonable values for the applied field and electrical polarization could not be extracted from the raw signal, because of electronic equipment failure.

Conclusions

1. Synthesis and chemical characterization:

Solid state reaction under HP-HT conditions (6 GPa and 950°C), and the hydrothermal method under HP-HT lead to practically single phase bulk $PbVO_3$ and $PbV_{1-x}M_xO_3$ (with M = Ti, Fe) compounds and $PbVO_3$ single crystals, respectively.

EDX method confirmed the nominal chemical composition of samples.

The knowledge of the oxidation states of V, M = Ti and Fe in $PbV_{1-x}M_xO_3$ is important for the explanation of the structural and magnetic properties of the samples.
XAS investigations show that the partial substitution with Ti is isovalent (in Ti substituted samples Vanadium is 4+ oxidized), but the substitution with Fe is not isovalent (for the substitution sample with x=25 % at. Fe a mixture of V^{4+} and V^{5+} was evidenced).

2. Structure:

XRD data and a combination of XRD and NPD data led to a refined structure of samples.

X-Ray diffraction (XRD) data show that $PbVO_3$ sample crystallizes on the tetragonal space group P4mm with the lattice parameters a = 3.79 Å and c = 4.66 Å.

After the isovalent substitution (V with Ti), the samples maintain the tetragonal symmetry for all the Ti concentrations.

The non-isovalent substitution (V with Fe) lead to the decrease of the tetragonality structure by increasing x, and above x=50% Fe substitution of V a new cubic phase appears.

By using anisotropic broadening of the Bragg peaks (observed for all samples) the uniaxial strain and size effects were calculated. The crystallites are compressed and subjected to strain along the c* direction. The strain effects are related to the presence of ferroelectric domains. The size effects were attributed to the reduced dimensions of coherent X-ray diffraction domains and to the increase of the number of defects.
Vanadium establishes a short vanadyl bond which places it on an off-centre distorted, 5 fold coordination, but Ti and Fe do not form an equivalent bond and hence tend to adopt a less distorted coordination.

3. Magnetic and dielectric properties:

The broad maximum of magnetic susceptibility vs. temperature for $PbVO_3$ and for sample with x=10% Ti is typical for 2D spin systems and the upturn at low temperatures is ascribed to the paramagnetic contribution of impurities and defects. The broad peak of the magnetic susceptibility curve is resonably fitted by the frustrated square lattice model (FSL).

In samples with Ti, the temperature dependence of the magnetic susceptibility is well fitted by using two contributions from 2D AFM model and from paramagnetic Curie-Weiss, respectively.

The fitting parameters (the decrease of the effective moment and Weiss temperature with increasing Ti content) reveal a decrease of the interactions between the magnetic moments, which is consistent with the dilution of magnetic moments.

The effect of partial substitution of V with Fe in $Pb(V_{1-x}Fe_x)O_3$ samples is the occurrence of both AFM and FM interactions (from temperature dependence of magnetic susceptibility measurements and the hysteresis in magnetisation curve). Specific heat measurements and NPD reveal no transition of any type. This suggests the formation of a spin glass system. The DC and AC susceptibility results also support the spin glass model. The formation of a spin glass system is explained by the disorder induced at the B site cation and by the different types of interactions between the magnetic cations.

The electrical resistivity for $PbVO_3$ single crystals yields a semiconductor behaviour with a gap energy of $E_A = 0.25 - 0.29$ eV.

An electric polarization hysteresis was evidenced for $PbVO_3$ single crystals confirming the ferroelectric nature of $PbVO_3$. However, the saturation value could not be reached.

For the $PbV_{0.6}Fe_{0.4}O_3$ compound measurements of dielectric constant indicate that the sample is a ferroelectric relaxor. The onset of the ferroelectric relaxor properties can be explained by inhomogeneities and local structural fluctuations which are caused by the disorder of the B site cations.

References

1. N. Hill, Why Are There so Few Magnetic Ferroelectrics?, *J. Phys. Chem. B*, *104,* 6694-6709, 2000.

2. J. Kreisel, Le défi du couplage entre magnétisme et ferroélectricité *Reflets de la Physique*, 2008, 8, 10.

3. L.W. Martin, Multiferroic and magnetoelectric heterostructures, *Acta Materialia*, 60, 2449–2470, 2012.

4. Eerenstein W., Multiferroic and magnetoelectric materials, *Nature*, 442:759, 2006.

5. C. Darie, Magnetic and crystal structures of BiCrO3, *Solid State Sciences,* 2009.

6. F. Kubel, H. Schmid, Structure of a Ferroelectric and Ferroelastic Monodomain Crystal of the Perovskite $BiFeO_3$, *Acta. Cryst.,* B 46, 698-702, 1990.

7. Yuichi Shimakawa, Multiferroic Compounds with Double-Perovskite Structures, *Materials*, *4*, 153-168, 2011.

8. K.F. Wang, J.M. Liu, Z.F. Ren, Multiferroicity: the coupling between magnetic and polarization orders, *Advances in Physics,* 58, 4, 321-448, 2009.

9. S-W. Cheong, M. Mostovoy, Multiferroics: A magnetic twist for ferroelectricity. *Nature Mater.,* 6, 13–20, 2007.

10. D. J. Singh, Polar Behavior in a Magnetic Perovskite from *A*-Site Size Disorder: A Density Functional Study, *Physical Review Letters*, 100, 087601, 2008.

11. G Lawes, G Srinivasan, Introduction to magnetoelectric coupling and multiferroic films, *J. Phys. D: Appl. Phys.*, 44, 243001, 2011.

12. Ponniah Ravindran, Magnetic-Instability-Induced Giant Magnetoelectric Coupling, *Adv. Mater.,* 20, 1353–1356, 2008.

13. P. Bordet, C. Bougerol, C. Brachet, S. de Brion, G. Chouteau, F. Hipper, J. Kreisel, << Recherche par Synthèse haute pression de Nouvelles Perovskites Multiferroïques de Type (Bi,Pb)MO_3, (M=métal de transition) >>, Meeting of the GDR NEEM, Aspet, France, 29 June-2 July 2004.

14. Roman V. Shpanchenko, Synthesis, Structure, and Properties of New Perovskite $PbVO_3$, *Chem. Mater.,* 16, 3267-3273**,** 2004.

15. Alexei A. Belik, Crystallographic Features and Tetragonal Phase Stability of $PbVO_3$, a New Member of $PbTiO_3$ Family, *Chem. Mater.,* 17, 269-273**,** 2005.

16. Alexander Tsirlin, Frustrated spin 1/2 square lattice in layered perovskite $PbVO_3$, *Physical Review B,* 77, 092402, 2008.

17. Kengo Oka, Magnetic Ground-State of Perovskite $PbVO_3$ with Large Tetragonal Distortion, *Inorg. Chem.,* 47, 7355-7359, 2008.

18. Angel Arevalo-Lopez, Miguel Alario-Franco, Structural Percolation in the $PbM_{1-x}M'_xO_3$ (M, M' =Ti, Cr, and V), *Perovskites Inorg. Chem.,* 50, 7136–7141, 2011.

19. Atahar Parveen, Thermal properties of a novel compound $PbVO_3$, *Journal of Physics: Conference Series,* 377, 012059, 2012.

20. Wei Zhou, Structural properties of $PbVO_3$ perovskites under hydrostatic pressure conditions up to 10.6 GPa, *J. Phys. Condens. Matter.*, 24, 435403, 2012.

21. H. Tracy Hall, Ultra-High-Pressure, High-Temperature Apparatus: the "Belt", *The Review of Scientific Instruments*, 31, 125-131, 1960.

22. L. G. Khvostantsev Vereshchagin L.F., Novikov A.P., Device of Toroid for high pressure generation, *High Temp. High Press.,* 9, 639-639, 1977.

23. C. Goujon, M. Legendre, A new differential thermal analysis setup for measuring high pressure phase transitions, *High Pressure Research,* 31, 375-387, 2011.

24. J.M. Cowley, Electron-Diffraction Study of the Structure of Basic Lead Carbonate, $2PbCO_3 \bullet Pb(OH)_2$, *Acta Cryst.,* 9, 391-396, 1956.

25. P. W. Stephens, Phenomenological model of anisotropic peak broadening in powder diffraction, *J. Appl. Cryst.,* 32, 281-289, 1999.

26. H. Rosner, High-temperature expansions for the J1-J2 Heisenberg models: Applications to *ab initio* calculated models for Li_2VOSiO_4 and Li_2VOGeO_4, *Physical Review B,* 67, 014416, 2003.

27. Yoshitaka Uratani, First principles on the Magnetic Anisotropy in Multiferroic $PbVO_3$ and $BiCoO_3$, *Journal of the Physical Society of Japan,* 78, 8, 084709, 2009.

28. Claire Laulhé Structure locale dans un ferroélectrique relaxeur: $BaTi_{1-x}Zr_xO_3$, 2007.

29. L.E. Cross, Ferroelectrics, 76, 241, 1987.

30. P. Neenu Lekshmi, Room temperature relaxor ferroelectricity and spin glass behavior in Sr_2FeTiO_6 double perovskite, *Journal of Alloys and Compounds*, 522, 90– 95, 2012.

31. Takeshi Tsuchiya, High-pressure synthesis and characterization of a novel perovskite $PbFe_{1/2}V_{1/2}O_3$, *Journal of Ceramic Society of Japan,* 117 [1] 102-105, 2009.

Acknowledgements

It is not just a duty and an honour, but also a great joy for me to give my acknowledgements to all of those who, one way or another have contributed to the conclusion of this work.

I feel honoured and indebt to express my respect and gratitude towards the entire team of true professionals which were my model to follow and towards the friends I made who were the shoulder upon which I relied.

A special tank you is reserved for Professor Dr. Aurel POP for the long hours of conversations and wonderful explanations needed for structuring the work and data interpretation, for the time and effort he invested, for the painstaking work, for his patience and for maintaining a good working atmosphere even when I made severe mistakes.

I would like to thank Professor Dr. Pierre BORDET for leading me through the basis of crystallography, refinements, computers and virtually every scientific (or not) topic I brought to discussion. I also thank him for the patience he has proven during the long hours of conversation.

Special thank you-s also go to Professor Dr. Claire COLIN who introduced me to practically every type of measurement that was ever conducted during this thesis, from the relatively simple ones (like the switching of electrical polarization), passing through the SQUID and going all the way to really sophisticated measurements (XAS or specific heat).

I would now like to step over to the microscopy side and send a special tank you to Professor Dr. Céline DARIE for introducing me to the wonderful Jeol SEM and for teaching me almost everything I know about using a SEM and trusting me. I also owe Professor Céline DARIE another thank you for the synthesis of our samples.

Again on the realm of crystallography, I would like to address a big thank you to Dr. Olivier LEYNAUD, for the patience he had while handling the cumbersome tiny $PbVO_3$ crystal, but also for the patience in showing me any mechanism I might have been interested on.

Of course I cannot forget to thank Professor Dr. Sébastien PAIRIS for teaching me with endless patience and understanding everything I know about the scanning electron microscopy, that I have not learned from Professor Céline DARIE.

There is yet one more microscopist, to whom I owe many, many, thank you-s, and I am talking here about Professor Dr. Stéphanie KODJIKIAN, who helped me overcome my fears of failure and introduced me to the electron diffraction technique.

I would also like to thank my other mentors on magnetization measurements, Dr. Eric EYRAUD and Dr. Didier DUFEU.

Stepping to the closely related field of measurements of dielectrical properties, I owe many thanks to Professor Dr. Jacques MARCUS and Professor Dr. Frédéric GAY, for the patience they had handing my delicate samples and for staying extra hours when I needed their help. I sincerely thank them for the effort. Following the same thread I would like to thank Dr. Jérôme DEBRAY for his much needed help at constructing mirror-like polished surfaces on sintered samples used during dielectric measurements.

I also want to thank Dr. Murielle LEGENDRE and Dr. Céline GOUJON for the effort they invested on repairing the HP-HT equipments over and over again. Without their hard work the research could not have been possible.

Another big thank you goes to Professor Dr. Pierre STROBEL for every synthesis that was not carried out under HP – HT conditions and for the help with chemistry related problems and annealing treatments.

I owe a big thank you to Professor Dr. Olivier ISNARD for handling the paperwork and the organizing problems.

A lot of effort was (and still is) invested on Mössbauer spectroscopy measurements and for this I express my gratitude to Professor Dr. Bernard MALAMAN.

I want to thank Prof. Dr. Laurent RANNO for the effort and long hours spent in the attempt to synthesize $PbVO_3$ thin film samples by using the PLD technique.

I am sincerely thankful to all the persons from the staff of the big instruments, the ILL and the ESRF, professors and engineers for their hard work and dedication, for their long, late, extra-hours spent supervising and programming the sophisticated instruments. Without their sacrifice we would have never obtained the answers we were seeking.

On the Romanian team I would like to thank Professor Dr. Viorel POP for introducing me to the French laboratory.

I sincerely thank professors Prof. Dr. Nicolae LEOPOLD and Prof. Dr. Vasile CHIS for their hard and stubborn work against the unmanageable Raman spectroscopy data.

Furthermore I would like to thank Professor Dr. Marin COLDEA for the strong interest manifested towards our research, interest that was matched by the help provided on the interpretation of magnetic measurements.

For further productive discussion and clarifications on the contradicting magnetic properties displayed by our samples I would like to bring a big thank you to Professor Dr. Iosif DEAC.

I am also deeply thankful to Professor Dr. Daniel ANDREICA for his interest and his efforts invested in the acquisition of new types of experimental data.

Also I would like to think Dr. Oana RAITA and Dr. Ovidiu PANA for their hard work at the acquisition and interpretation of EPR data and other data which shed a new light on the subject of $PbVO_3$ and open the door on new perspectives of research on this material.

Lastly, I cannot forget to thank Dr. Daniel MARCONI for good advices and practical help in bringing the work to its final form.

For all the things mentioned I thank everybody one more time. And one other thing, equally important: I thank all for the trust they bestowed in me (although there were some moments which did not fully justified it), for the patience they had with me, and the understanding they proved, even during tensioned and stressful moments; for their encouragements, for their scolding, for all they gave me, for all they took from me, for all I have stolen from them, because I have seen and understood side by side with them what team work means and what research means and what is the meaning of a common purpose.

Paraphrasing Antoine de Saint-Exupéry who used to say: “Aimer, n’est pas se regarder l’un l’autre, mais regarder tous les deux dans la même direction” I can certainly say that I am a privileged of fate because I had the chance to watch in the same direction with my mentors in the field of research, even for an, unfortunately limited, period of time.

List of publications and conferences

Publications:

1. Alexandru Okos, Aurel Pop, Céline Darie, Pierre Bordet, High pressure - high temperature synthesis and phase characterization of $PbVO_3$ perovskite compound, STUDIA UBB CHEMIA, LVIII, 3, p 57-62, 2013.

2. Alexandru Okos, Aurel Pop, Céline Darie, Pierre Bordet, Crystal structures and microstrucutres of $PbV_{1-x}Fe_xO_3$ perovskites with $x \leq 0.3$, accepted for publication in Optoelectronics and Advanced Materials.

3. Alexandru Okos, Aurel Pop, Céline Darie, Pierre Bordet, The influence of partial substitution of V with Fe on structure, phase purity and microstructure of the multiferroic $Pb(V_{1-x}Fe_x)O_3$ compound, accepted for publication in STUDIA UBB PHYSICA.

Conferences:

1. Alexandru Okos, Claire V. Colin, Murielle Legendre, Olivier Leynaud, Sébastien Pairis, Aurel Pop, Pierre Bordet and Céline Darie, "Synthèse haute pression, structure, propriétés physiques de $Pb(V,A)O_3$, A = Fe,Ti", 13-ième Journées de la Matière Condensée (JMC 13), Montpellier 27-31 Août 2012.